IEEE Access
Multidisciplinary | Rapid Review | Open Access Journal

Received April 22, 2020, accepted May 9, 2020, date of publication May 14, 2020, date of current version June 9, 2020.

Digital Object Identifier 10.1109/ACCESS.2020.2994323

Optimization and Performance Evaluation of a Transducer for Bone Conduction Implants

SEUNG HYUN LEE[1], KI WOONG SEONG[2], KYU-YUP LEE[3], AND DONG HO SHIN[4]

[1]College of Health Science, Institute of Global Health Technology, Korea University, Seoul 02841, South Korea
[2]Department of Biomedical Engineering, Kyungpook National University Hospital, Daegu 41944, South Korea
[3]Department of Otorhinolaryngology-Head and Neck Surgery, School of Medicine, Kyungpook National University, Daegu 41944, South Korea
[4]Institute of Biomedical Engineering Research, Kyungpook National University, Daegu 41944, South Korea

Corresponding author: Dong Ho Shin (swap9552@naver.com)

This work was supported in part by the Korea Health Industry Development Institute (KHIDI) through the Korea Health Technology Research and Development Project, funded by the Ministry of Health and Welfare, South Korea, under Grant HI18C1892, and in part by the National Research Foundation of Korea (NRF) grant funded by the Korean Government (MSIP) under Grant NRF-2019R1C1C1006176 and Grant NRF-2019R1C1C1011408.

ABSTRACT We designed and implemented an electromagnetic transducer for implantable bone conduction hearing aids. The proposed transducer is smaller than previous bone conduction transducers for easy implantation and was designed using high permeability metals to produce large electromagnetic forces. In addition, the number of cantilever beams was changed from two to three to minimize distortion of the transducer, potentially due to twisting of the cantilever beam. The proposed transducer consists of a titanium cover with three screw holes, a metal ring, a circular plate, a vibrational membrane with a three-cantilever structure, a metal plate and cylinder, a permanent magnet, top and bottom coils, and a cylindrical titanium case. The transducer was optimally designed based on analysis of electromagnetic and mechanical vibrations, and the target resonance frequency was derived by controlling the variable elements of the vibrational membrane. The transducer was manufactured based on the results of finite element analysis, and the validity of the design was verified by comparing the results of vibration measurement experiments and a simulation. Finally, to evaluate the performance of the proposed transducer, the transducer was attached to the mastoid of participants and functional near-infrared spectroscopy was used to measure brain activation changes of the auditory cortex due to vibration stimulation.

INDEX TERMS Implantable bone conduction hearing aid, electromagnetic transducer, finite element analysis, functional near-infrared spectroscopy.

I. INTRODUCTION

Thus far, various types of hearing aids have been developed to treat hearing loss. Such hearing aids can be divided into air conduction hearing aids, middle-ear implants, and cochlear implants, depending on the application position [1]–[7]. Air conduction hearing aids with sound pressure output, which are most commonly used for treatment of hearing loss, are advantageous in that surgery is not required; however, they have disadvantages such as acoustic feedback and occlusion of the ear canal [8], [9]. Middle-ear implant hearing aids use small transducers to transmit vibration corresponding to sound directly to the ossicular chain or round window; these transducers are advantageous in they reproduce natural sound without any acoustic feedback. Because middle-ear implants require complicated surgery, they are not a popular choice for many patients with hearing loss. In addition, they are difficult to apply if the ossicular chain is lost due to disease or is anomalous [10]–[14]. Cochlear implantation is the only method to restore hearing to patients with severe-to-profound sensorineural hearing loss; indications for cochlear implantation differ greatly from the indications for hearing rehabilitation systems listed above. In addition, cochlear implantation involves complex surgery [15]–[17].

Recently, implantable bone conduction hearing aids, which can partially compensate for the disadvantages of conventional hearing aids and can be implanted with minimally invasive procedures, have been developed and used in clinical research [18]–[21]. Bone conduction hearing aids use an output device (e.g., a transducer) that generates vibration in

The associate editor coordinating the review of this manuscript and approving it for publication was Wenbing Zhao.

the same manner as a conventional middle ear implantable hearing aid; it transmits a vibration signal corresponding to sound by means of bone conduction via implantation of a transducer into the mastoid [22]. The vibrational signal of the transducer causes considerable loss of the vibration signal during propagation through media, such as skin and bone. Thus, there is a need for the development of transducers that produce high vibration outputs.

Shin *et al.* [23] proposed and developed a prototype of a dual-coil transducer for bone conduction hearing aids. The transducer is 18 mm in diameter and 11 mm in height, with a mechanical resonance frequency of 1.2 kHz. However, the prototype transducer was not optimized for use as an implantable bone conduction transducer in terms of its size and frequency characteristics. Therefore, it is necessary to miniaturize the transducer for easy implantation. In addition, to compensate for conductive hearing loss, improvement of the frequency characteristics and vibration force of the transducer is required.

In this study, a transducer was designed based on electromagnetic and mechanical vibration analysis to miniaturize transducers and control resonant frequencies. To minimize the distortion caused when the transducer is operating, the number of cantilever beams of the vibrational membrane was changed from two to three. In addition, the reduction of vibrational force due to miniaturization was compensated by using the magnetic yoke as a high permeability metal. The transducers were fabricated based on simulation results, and the validity of the design was verified by performing vibration measurement experiments under no-load conditions.

Generally, transducers for implantable hearing aids in early stages of development are assessed for performance through nonclinical studies, such as cadaveric experiments using human temporal bone. However, these nonclinical experiments cannot assess whether a patient perceives sound, in terms of brain activation. Recently, neuroimaging studies on auditory cortex have been conducted using functional magnetic resonance imaging (fMRI) [24], [25]. Because the electromagnetic transducers proposed in this study contain permanent magnets, neuroimaging studies using fMRI are difficult. In contrast, functional near infrared spectroscopy (fNIRS) can be used to measure changes in brain activation of the auditory cortex without being affected by permanent magnets [26]–[29]. Therefore, performance evaluation was conducted using fNIRS for the electromagnetic type bone conduction transducer proposed in this study.

II. DESIGN OF THE TRANSDUCER

A. STRUCTURE OF THE TRANSDUCER

An implantable bone conduction hearing aid is composed of an external device including a microphone, as well as an internal device including a signal processing module and a transducer, as shown in Fig.1. The bone conduction hearing aid works by transmitting sound vibrations through the bone using the transducer. The inner ear receives sound vibrations and converts sound vibrations into electrical signals that the brain interprets as sound. Therefore, the bone conduction hearing device allows a patient with hearing loss to hear sounds that cannot pass through the ear in the normal manner. Typically, transducers in implantable bone conduction hearing aids are implanted in the mastoid region. However, the vibrational signal generated by the transducer is propagated through the bone, which leads to a high level of loss. Therefore, considering the lost vibrational signal, the transducer must be able to produce a high output.

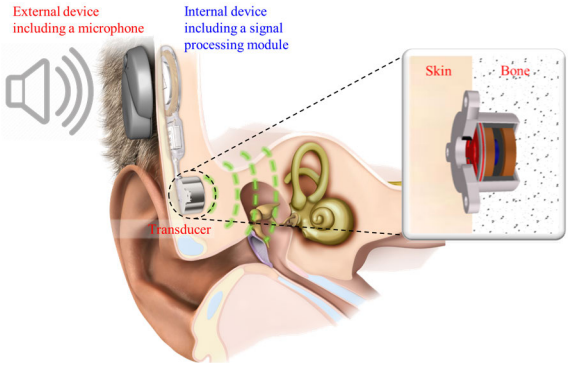

FIGURE 1. Conceptual schematic diagram of implantable bone conduction hearing device [23], [30].

In this paper, vibrational force improvement studies were performed, along with optimal size derivation of the transducer to be used as an output device for implantable bone conduction hearing aids. The dimensions of the transducer were set based on the BONEBRIDGE BCI-601 (Med-El, Innsbruck, Austria) and computed tomography image of the cranium [30]. The proposed transducer has a diameter of 15 mm and a height of 10 mm, 8 mm of which is implanted into the bone. The transducer consists of a titanium cover with three screw holes (for fixation of the transducer to the bone), a metal ring (for fixation of the membrane), a circular plate (for connection of the vibrational membrane with the permanent magnet), a vibrational membrane with a three-cantilever structure (for generation of mechanical resonance), a metal plate and cylinder (for maximization of magnetic density), a permanent magnet, top and bottom coils wound in opposite directions, and a cylindrical titanium case, as shown in Fig. 2.

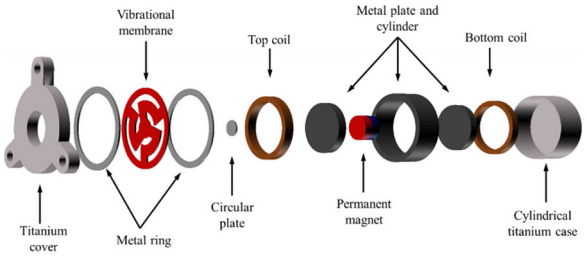

FIGURE 2. Part list of bone conduction transducer.

The proposed bone conduction transducer can be expressed as single-degree-of-freedom (SDOF) system composed of a

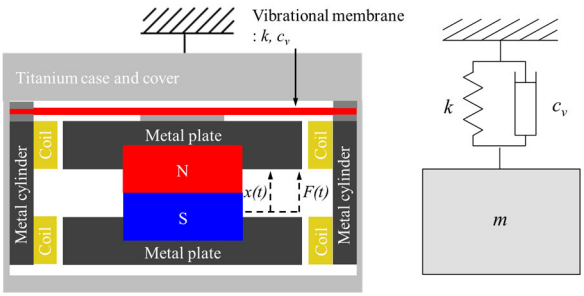

FIGURE 3. Single-degree-of freedom systems of bone conduction transducer.

mass (m), a spring (k) and viscous damping (c_v) (Fig. 3). However, viscous damping was not considered in the motion equations, because viscous damping from the air is low. The motion equation of the SDOF system is as given in Eq. (1); this equation can be used to theoretically derive the magnitude of the vibration displacement of the transducer [31], [32].

$$m\ddot{x}\,(t) + kx\,(t) = Fsin\omega\,(t) \tag{1}$$

Here, m is the total mass of the permanent magnet and the circular metal plate, k is the stiffness of the vibrational membrane, F is the electromagnetic force generated by the permanent magnet and coils when the current flows, and ω is the angular frequency.

The actual displacement (X) of the bone conduction transducer with SDOF derived from Eq. (1) is:

$$X = \frac{F}{\left(k - m\omega^2\right)}[\mathrm{m}] \tag{2}$$

and the mechanical resonance frequency of the bone conduction transducer can be calculated using the following equation.

$$\omega_n = \sqrt{\frac{k}{m}}[\mathrm{Hz}], \quad \omega_n : \text{resonance frequency} \tag{3}$$

Using the equations defined above, an approximate theoretical value can be obtained for the vibration displacement of the transducer. However, the electromagnetic force used in the equation is generated by interlinkage of the flux of the permanent magnet and the flux generated when the current flows through the coils; thus, mathematical derivation of the magnitude of electromagnetic force is very complicated. In addition, it is difficult to derive the exact value of the vibration displacement. Therefore, electromagnetic analysis and mechanical vibration analysis were performed using finite element analysis (FEA) software for simplicity.

B. ELECTROMAGNETIC ANALYSIS

As an output device for implantable hearing aids, transducers with high efficiency are required, because batteries used in implantable hearing aids exhibit limited size and capacity.

In this paper, to increase the efficiency of the bone conduction transducer proposed by Shin *et al*. [23], the magnetic yoke using stainless steel 304 (SUS304) is replaced with a high permeability metal, such as Mu-metal. Subsequently, the magnitude of the Lorentz force calculated by electromagnetic analysis was compared with that of the conventional bone conduction transducer.

To obtain the maximum Lorentz force of the proposed bone conduction transducer, electromagnetic analysis was performed using the FEA software COMSOL Multiphysics 5.4 (COMSOL Inc., Stockholm, Sweden). Lorentz forces are generated by the interaction of magnets and coils; therefore, the vibrational membrane, metal ring, circular plate and titanium case (including the cover) were excluded, as they do not affect the analysis. To derive the maximum Lorentz force of the transducer, the simulation was performed with changing coil height from 1 mm to 3 mm in 0.1 mm increments. Here, considering the process of transducer assembly and the ease of manufacturing the metal plate, the gap between the metal and the coil was set to 0.1 mm; the magnet size was fixed at a diameter of 5 mm and a height of 4 mm. Considering the battery voltage used in the implantable bone conduction hearing aid, the current applied to the coil was set to 8 mA@0 kHz; the implantable bone conduction hearing aid undergoing analysis at Kyungpook National University Hospital uses a battery voltage of 3 Vp. In addition, the thickness of the coil was fixed at 0.051 mm, based on the standard specification of the self-bonding coil used for winding. The two-dimensional axisymmetric model used for electromagnetic analysis is shown in Fig. 4(a); Fig. 4(b) shows the results of electromagnetic analysis and indicates the magnetic flux density arising from the permanent magnet and coils. Fig. 4(c) shows Lorentz forces according to the height of the coil. The analysis results demonstrated that the maximum Lorentz force of 587 mN was generated when the coil height was 3 mm. However, at a coil height of 3 mm, the total resistance is approximately 550 Ω, and it is difficult to apply a current equivalent to 8 mA@0 kHz with the battery voltage. Therefore, the maximum coil height of the proposed transducer was set at 2 mm and the Lorentz force generated at this height was approximately 486.4 mN. The values of the parameters of the transducer components for generating the maximum Lorentz force are as follows. All components of the transducer were established using the magnetic field routine of the AC/DC module, and then combined using the "form union" command. The surface gauss of the permanent magnet (NdFeB, grade N35AH) with a diameter of 5 mm and height of 4 mm is 0.43 T. Each coil has an outer diameter of 12.2 mm, inner diameter of 10.2 mm, height of 2 mm, and thickness of 0.051 mm, with 600 turns and a resistance of 180 Ω. Here, a "homogenized multi-turn" coil conductor model was used; the coil excitation was "current" and the coil wire conductivity was $4.3e^7$ [S/m]. The windings of the top and bottom coils were set to be in opposite directions to each other; a current corresponding to 8 mA@0 kHz was then applied to the coils. To minimize the leakage of magnetic flux

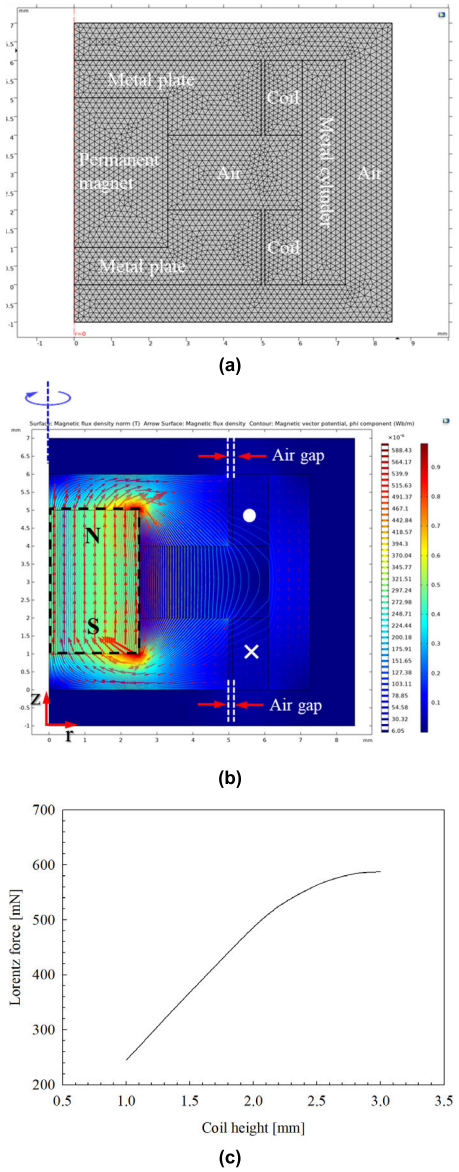

FIGURE 4. **(a) Two-dimensional axisymmetric mesh model, (b) analysis of magnetic flux density by permanent magnet and coils, and (c) Lorentz forces according to height of coil.**

generated from the permanent magnets, a metal plate (diameter 10 mm and height 2 mm) and a metal cylinder (outer diameter 14.5 mm, inner diameter 12.2 mm, and height 6 mm) made of Mu-metal (relative permeability of 20,000, electrical conductivity of $1.67e^4$ [S/m], relative permittivity of 1) were used. The mesh type of the two-dimensional axisymmetric model was set to ''free triangular''. The element parameters of the mesh include a maximum element size of 0.17 mm, minimum element size of 0.000637 mm, maximum element growth rate of 1.2, curvature factor of 0.25, and narrow region resolution of 1. The mesh model consisted of 6,495 domain elements and 509 boundary elements.

To compare whether the structure using high permeability metal has higher efficiency than the SUS304 structure used by Shin *et al.*, Mu-metal was changed to SUS304 (relative permeability of 1.008, electrical conductivity of $1.39e^7$ [S/m], relative permittivity of 1) in the same structure. An electromagnetic analysis was then performed, and the maximum Lorentz force was approximately 385.4 mN. Comparing the two results, the use of Mu-metal led to approximately 20% greater Lorentz force, compared to that of SUS304.

C. MECHANICAL VIBRATION ANALYSIS

Mechanical vibration analysis was performed to determine the optimal frequency characteristics of the bone conduction transducer, based on the maximum Lorentz force derived from electromagnetic analysis. In general, the mechanical resonance of an implantable bone conduction device is between 0.7 and 1 kHz [33]. Therefore, the mechanical resonance frequency target of the bone conduction transducer proposed in this paper was designed to occur at 0.9 kHz. The mechanical resonance frequency of the transducer is determined by the stiffness of the vibrational membrane and the mass contributing to the vibrational membrane, as shown in Eq. (3). However, it can be difficult to control the mechanical resonance of the transducer due to the mass (sum of mass of metal plates and magnet) that contributes to the vibrational membrane. Therefore, the mechanical resonance of the transducer was controlled by adjusting the stiffness of the vibrational membrane. To easily control the rigidity of the vibration membrane, a vibration membrane with a cantilever structure was used. The stiffness of the vibrational membrane can be controlled by variable factors such as the width, thickness, angle (length), and number of cantilever beams. In this study, considering the miniaturization of the transducer and the wet etching process of the vibrational membrane, the beam thickness and width were fixed at 0.3 and 0.2 mm, respectively; the number of beams was fixed at three to minimize distortion. As it moves up and down in the metal cylinder, the magnet tends to move toward the inside wall surface of the cylinder. When there are two beams, there is a high probability that a ''rolling'' phenomenon will occur, leading to distortion of the transducer. However, when the number of beams is fixed at three, the rolling of the magnets is minimized and distortion is reduced. Then, the beam angle alone was used to adjust the stiffness of the vibrational membrane. Fig. 5 shows the structure of the vibrational membrane proposed to generate the mechanical resonance of the bone conduction transducer, with the three beams located between the stationary ring and the plate.

The 3D mesh model used in the analysis is shown in Fig. 6 (a); mechanical vibration analysis was performed to determine the optimal frequency characteristics of the bone conduction transducer. The 3D model only represented the mass components (including the magnet, metal plates, and circular plate) that affect the vibrational membrane without being anchored to the bone, as well as the vibrational membrane with the cantilever structure required for mechanical vibration analysis. All components in the 3D model were configured using the solid mechanics routine of the

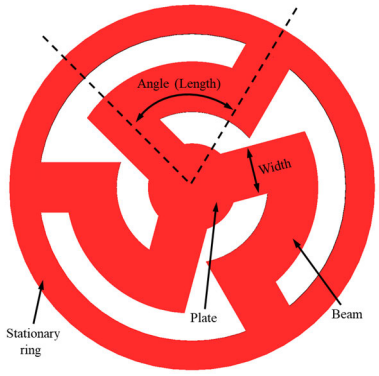

FIGURE 5. Shape of vibrational membrane with cantilever structure.

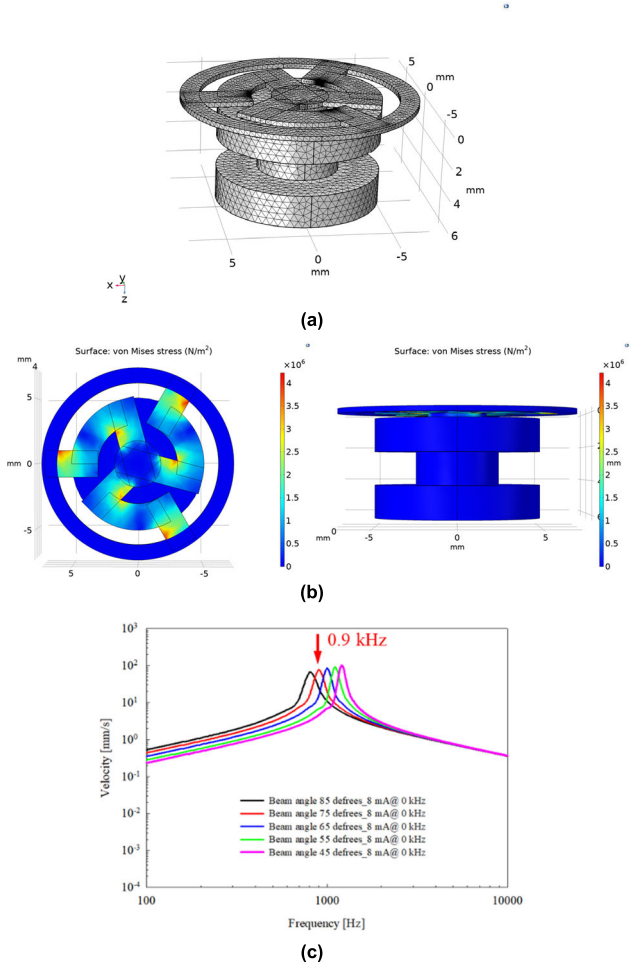

FIGURE 6. (a) Three-dimensional mesh model for mechanical vibration analysis, (b) distribution of von Mises stress (top and side view) based on the static analysis, and (c) frequency response characteristics according to beam angle based on the dynamic analysis.

structure mechanics sub-module, then combined with the ''form union'' command. The stationary ring of the vibrational membrane was fixed using a defined ''fixed constraint''. The prescribed displacements of the permanent magnet, two metal plates, and beams of the vibrational membrane were set to ''free/free'' [10]. The total force of the body load applied to the permanent magnet and two metal plates during mechanical vibration analysis was 486.4 mN (previously calculated by electromagnetic analysis); the total mass applied to the vibrational membrane was 2.77 g (2.2 g of metal plates and 0.57 g of permanent magnet). The mesh type of the 3D model was set to ''free tetrahedral''. The element parameters of the mesh include a maximum element size of 0.508 mm, minimum element size of 0.0218 mm, maximum element growth rate of 1.35, curvature factor of 0.3, and narrow region resolution of 0.85. The mesh model consisted of 88,269 domain elements, 19,977 boundary elements, and 2,251 edge elements. The vibration analysis was performed by changing the angle of the beam from 45° to 85° in 10° increments. The distribution of von Mises stress, which represents the maximum distortion energy density at each measurement point under load (based on the static analysis result), and the frequency response characteristics according to the beam angle (based on the dynamic analysis result), are shown in Fig. 6(b) and 6(c), respectively. The critical stress of the vibrational membrane based on the static analysis results is $5.18e^6$ N/m^2. As shown in Fig. 6(c), when the beam angle is 75°, the proposed transducer can generate a mechanical resonance frequency at 0.9 kHz.

III. RESULTS

A. IMPLEMENTATION OF THE TRANSDUCER

The optimal design of the bone conduction transducer was established by means of electromagnetic and mechanical vibration analysis, and the bone conduction transducer was fabricated based on the analysis results. Each component of the bone conduction transducer was fabricated using CNC machining processes and wet etching. The vibrational membrane, circular plate, and metal ring were fabricated using a photochemical technique (a wet etching method). A masking film was produced using CAM350 software, and a dry film photoresist was attached to stainless steel 316 (SUS316) using a laminator. The masking film was patterned on SUS316 using an exposure process (ultraviolet transmission); then, the patterned SUS316 was etched using ferric chloride solution ($FeCl_3$). At this time, the temperature of the solution was 40–50° and the etching duration was 20–30 minutes. Finally, the vibration membrane (diameter, 14.5 mm; angle, 75°; thickness, 0.3 mm), circular plate (diameter, 3.5 mm; thickness, 0.2 mm), and metal ring (outer diameter, 14.5 mm; inner diameter, 12.2 mm; thickness, 0.2 mm) were completed through a stripping process using sodium hydroxide solution (NaOH). The metal cylinder (outer diameter 14.5 mm, inner diameter 12.2 mm, and height 6 mm, Mu-metal), two metal plates (diameter 10 mm and height 2 mm, Mu-metal), cylindrical titanium case (outer diameter 15 mm, inner diameter 14.5 mm, and height 8 mm, Ti-6Al-4V), and a titanium cover with three screw holes (diameter 16 mm and height 2 mm, Ti-6Al-4V) were machined using a CNC machining processes. Each coil (outer diameter 12.2 mm, inner diameter 10.2 mm, and height 2 mm) was wound 600 turns using an automatic winding machine. The

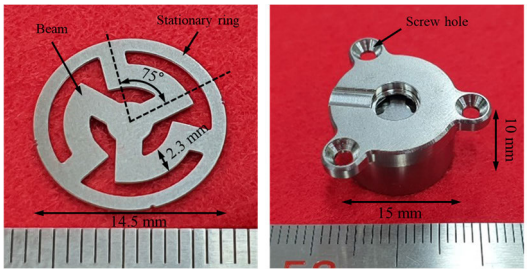

FIGURE 7. **Manufactured vibrational membrane and assembled bone conduction transducer.**

permanent magnet (diameter 5 mm and height 4 mm, NdFeB, grade N35AH) was custom-made to ensure that no magnetic force was lost, even at temperatures above 200°. Each component of the bone conduction transducer was assembled using epoxy on a probe station equipped with a microscope. When assembling, the two metal rings and the stationary ring of the vibrational membrane were firmly fixed to the cylindrical titanium case. Therefore, when the outside of the cylindrical titanium case is firmly fixed to the bone, it is assembled to operate only the magnet, metal plate, and beam of the vibration membrane inside the transducer. Fig. 7 shows the manufactured vibrational membrane and assembled bone conduction transducer.

B. FREQUENCY RESPONSE CHARACTERISTICS

To confirm the frequency response characteristics of the fabricated bone conduction transducer, vibration characteristics were measured under no-load conditions. As shown in Fig. 8(a), vibration measurements were performed using a laser Doppler effect-based laser Doppler vibrometer (OFV-5000, vibrometer controller; OFV-534, interferometer sensor head; Polytec GmbH, Germany) system and a Fast Fourier Transform-based data acquisition system (Fast Fourier Transform length: 4096, sampling rate: 96 kHz, average: 10, DAQ; NI PXIe-1071, NI PXIe-8840, and NI PXI-4461; National Instruments Co., USA). The system generates a sinusoidal signal to drive the bone conduction transducer while simultaneously storing the transducer's vibration signal, as measured by the laser Doppler effect-based laser Doppler vibrometer. To measure the vibration characteristics of the vibrational membrane, the bottom of the titanium case was firmly fixed to the anti-vibration table using epoxy, similar to the instance where the bone conduction transducer was fixed to the bone. The angle of incidence of the laser beam was then positioned perpendicular to the center of the vibrating membrane. After a current of 8 mA@0 kHz was applied to the bone conduction transducer, the frequency response was measured; the result is shown in Fig. 8(b). The fabricated transducer generated mechanical resonance at 0.9 kHz. When the measurement results were compared with the FEA results, there was a slight difference in the low- and high-frequency regions. This is likely due to the tolerance caused by using glue and the misalignment of components that occurs when

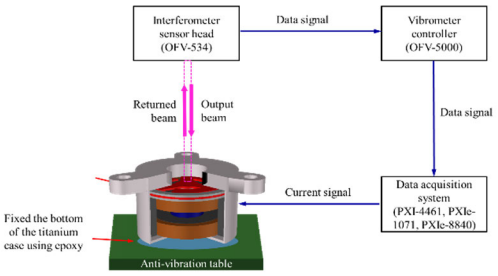

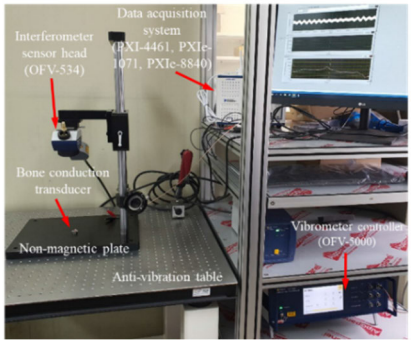

(a)

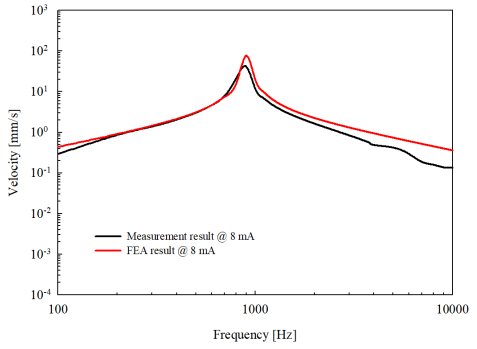

(b)

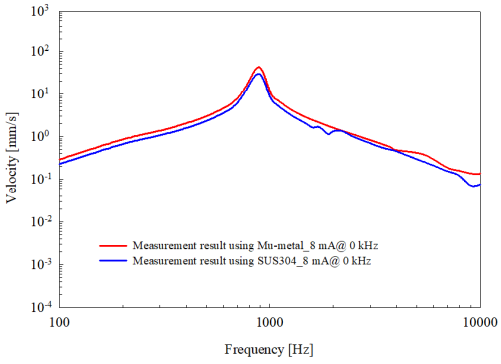

(c)

FIGURE 8. **(a) Block diagram and photograph of the experimental setup for vibration measurement, (b) comparison of the frequency response between the measurement and FEA results, and (c) comparison of output magnitude between SUS304 and Mu-metal transducers.**

assembling at the laboratory level. These problems could be solved in future by using laser welding and precision assembly machinery. Nevertheless, the shape and magnitude of the overall frequency characteristics were similar. In addition,

to verify the electromagnetic analysis result, it was compared with the frequency response measured using SUS304 (blue solid line). This transducer was manufactured in the same way as the Mu-metal transducer, except that the metal plate and cylinder were SUS304. The measurement results are as shown in Fig. 8(c); in comparison with the frequency response characteristics for Mu-metal (red solid line), the output magnitude of all frequency bands was reduced by around 25%.

IV. DISCUSSION

In general, transducers developed for use in implantable hearing aids are evaluated for performance by means of cadaveric experiments. However, the most accurate method is measurement of the auditory cortex response by means of transducer stimulation. The response of the auditory cortex can be measured using a technique such as fMRI. However, the bone conduction transducer proposed in this paper is composed of a permanent magnet and high permeability metal; therefore, fMRI is unsuitable for measurement with this transducer. Recently, the use of a novel neuroimaging approach, known as fNIRS, for measurement of auditory cortex activity has attracted attention in the field of auditory diagnosis [34], [35]. fNIRS is an emerging technique that can measure relative changes in concentrations of oxygenated hemoglobin and deoxygenated hemoglobin due to nerve activity. fNIRS is relatively small, portable, and non-invasive; it also exhibits a relatively high time resolution and artifact robustness, compared to fMRI [36]. Furthermore, fNIRS uses an optical fiber electrode; thus, it can be used to analyze a transducer containing a permanent magnet.

Therefore, in this study, an auditory cortex response experiment was performed using fNIRS technology to more clearly evaluate the performance of the proposed bone conduction transducer. To confirm whether the proposed transducer functions well as a hearing aid transducer, the auditory cortex response, based on same frequency stimulation, was measured using a kernel-type earphone and the proposed transducer. Ten healthy volunteers with no history of neurological, physical, or mental illness participated in this study. The study was approved by the Institutional Review Board of DGIST (DGIST-190724-HR-068-01); all participants provided written informed consent prior to the study.

Auditory stimulation using a kernel-type earphone was first performed; the bone stimulation experiment with the proposed transducer was then performed. Auditory stimulation using the kernel-type earphone was presented to the right ear; the left ear was shielded with earplugs to block incoming sound. For comparative analysis of the auditory cortex response, a bone stimulation experiment was conducted using the proposed transducer. The proposed transducer was attached near the mastoid, based on the actual implantation position. To bring the bottom of the transducer as close to the skull as possible, a self-adhesive elastic bandage (with length and circumference equivalent to the participant's head) was wrapped over the transducer; both ears were shielded with earplugs to block incoming sound. The frequency of sound for auditory stimulation was presented at 500 Hz, 1 kHz, 1.5 kHz, 2 kHz, and 4 kHz; the stimulus orders were randomly assigned for all participants. The hemodynamic response was then measured to assess the effects of pure tone auditory stimulation using an fNIRS system (LABNIRS, Shimadzu Corp., Kyoto, Japan). The experiments were arranged in a block paradigm. The block design consisted of 18 rest periods and 15 task periods. Each frequency was presented three times in one task trial. The auditory stimulation lasted for 20 seconds; after the end of the stimulation, there was a rest period of between 23 and 27 seconds to minimize phase synchronization for the stimulus (Fig. 9(a)).

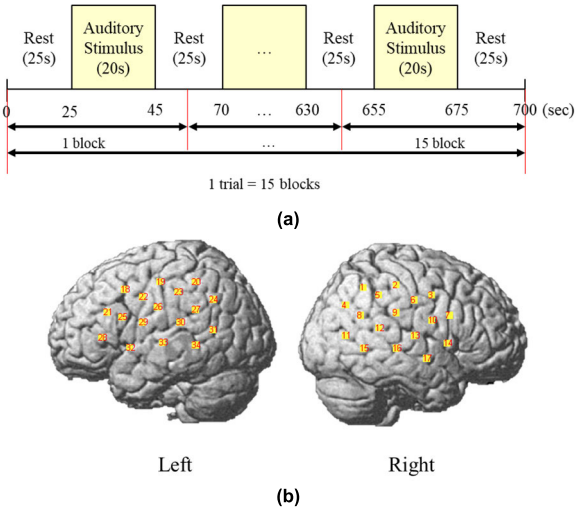

FIGURE 9. Configuration and cortical position of fNIRS experimental protocol: (a) experimental protocol and (b) configuration of fNIRS optodes.

The fNIRS signal was recorded in the auditory cortex on the participants' left and right hemispheres. Based on the 10-20 international electrode placement system, 12 optodes (6 transmitters and 6 receivers) were placed in the left and right hearing areas, respectively. The left auditory cortex is at approximately the T3 position and the right auditory cortex is at approximately the T4 position [37]. A total of 34 channels contained information regarding concentration changes in oxygenated hemoglobin (Fig. 9(b)). The measured fNIRS data included various artifacts, related to blood pressure, physiological changes in the participant, or device instability. Hemodynamic response functions and a wavelet-minimum description length detrending algorithm [38] were used to eliminate artifacts and improve signal-to-noise ratios. fNIRS data analysis was performed using the NIRS-SPM software package implemented in MATLAB (MathWorks, Inc., Natick, MA, USA) [39].

Fig. 10(a) and (b) show the cortical activation maps of oxygenated hemoglobin for the respective conditions of listening to the pure tone using a bone conduction transducer and using earphones. Both cortical activation maps showed a statistically significant difference in the auditory cortex. When using

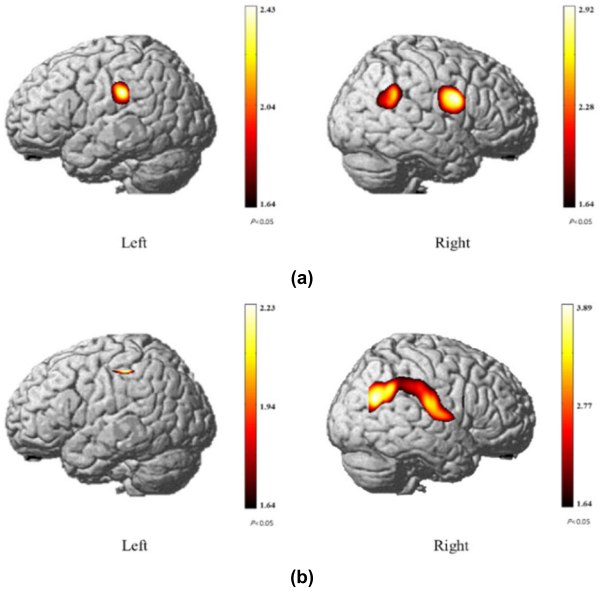

FIGURE 10. Cortical activation maps of oxygenated hemoglobin when listening to a pure-tone sound: (a) air conduction stimulation by kernel-type earphone and (b) bone conduction stimulation by proposed transducer.

a bone conduction transducer in the oxygenated hemoglobin group analysis, the auditory stimulation of the right ear led to activation of the right auditory cortex, while less activation was observed in the left auditory cortex. When using the earphones, significant activation was observed within bilateral auditory cortex.

The study was designed to observe brain activation patterns in the auditory area when using bone conduction transducers. In pure tone auditory stimulation, differences were observed between the bone conduction transducer and earphones in terms of lateralization of activity in the region of interest; however, the bone conduction transducer induced auditory cortex activation similar to the use of earphones.

V. CONCLUSION

This study investigated improvement of output characteristics and miniaturization on a bone conduction transducer previously proposed by Shin *et al*. Improvement experiments derived optimal parameters based on FEA, such as electromagnetic analysis and mechanical vibration analysis. The proposed transducer was implemented based on the FEA analysis, and the validity of the design was confirmed by comparing the analysis results with the frequency response characteristics of the transducer manufactured under no-load conditions. The FEA and experimental results obtained in this study are compared with the specific characteristics of the previous transducer, as shown in Table 1.

Consequently, the Lorentz force of the proposed transducer using high permeability metal produced a Lorentz force approximately 20% higher than that of the previous transducer. In addition, the volume of the proposed transducer was reduced by approximately 37% compared to the previous transducer, thereby facilitating implantation. In other words,

TABLE 1. Comparison of the proposed and previous transducers with the same current.

	Volume (cc)	Metal yoke material	Lorenz force (mN)	Average output magnitude (mm/s)
Previous transducer structure	2.79	Stainless steel 304	385.4	2.84
Proposed transducer structure	1.76	Mu-metal	486.4	3.81

considering the transducer alone, if its efficiency improves by 20%, the battery life is increased by the same amount However, from the point of view of the hearing aid system, it is necessary to consider the power transmission efficiency of the inductive link, and the battery power consumed by the peripherals of the external device. However, since the largest amount of power is consumed by the transducer, increasing the efficiency thereof can greatly extend the battery life.

Finally, to verify the performance of the proposed transducer, the auditory cortex response to bone stimulation was measured using the fNIRS technique. Then, the measured results were compared with the auditory cortical response results according to auditory stimuli using kernel-type earphones. The study confirmed that the bone conduction transducer activates the auditory cortex to which auditory stimulation is applied, similar to earphones. Therefore, this result is meaningful because it clearly demonstrates that bone conduction transducers activate the auditory cortex; it also demonstrates the validity of using fNIRS to assess the performance of a bone conduction transducer system.

Further research is needed to develop a mechanism to enhance the vibrational force of the transducer. A simulation study on the vibration transmission characteristics of the transducer is needed based on the skull and temporal bone.

REFERENCES

[1] R. L. Goode, M. L. Rosenbaum, and A. J. Maniglia, "The history and development of the implantable hearing aid," *Otolaryngol. Clinics North Amer.*, vol. 28, no. 1, pp. 1–16, Feb. 1995.

[2] D. S. Haynes, J. A. Young, G. B. Wanna, and M. E. Glasscock, "Middle ear implantable hearing devices: An overview," *Trends Amplification*, vol. 13, no. 3, pp. 206–214, Sep. 2009.

[3] G. Bernardi, T. Van Waterschoot, M. Moonen, J. Wouters, M. Hillbratt, and N. Verhaert, "Measurement and analysis of feedback and nonlinearities for the codacs direct acoustic cochlear implant," *IEEE Access*, vol. 5, pp. 8702–8713, 2017.

[4] L. Lassaletta, I. Sánchez-Cuadrado, J. M. Espinosa, Á. Batuecas, C. Cenjor, M. J. Lavilla, L. Cavallé, A. Huarte, F. Nuñez. M. Manrique, Á. Ramos, C. de Paula, and E. Gil-Carcedo, "Active Middle Ear Implants," *Acta Otorrinolaringol. (English Ed.)*, vol. 70, no. 2, pp. 112–118, Mar. 2019.

[5] R. M. Rhodes and B. S. Tsai Do, "Future of implantable auditory devices," *Otolaryngologic Clinics North Amer.*, vol. 52, no. 2, pp. 363–378, Apr. 2019.

[6] D. Calero, S. Paul, A. Gesing, F. Alves, and J. A. Cordioli, "A technical review and evaluation of implantable sensors for hearing devices," *Biomed. Eng. OnLine*, vol. 17, no. 1, pp. 1–26, Dec. 2018.

[7] M. Tisch, "Implantierbare Hörsysteme implantable hearing devices," *Laryngo-Rhino-Otologie*, vol. 96, no. S01, pp. S84–S102, Apr. 2017.
[8] A. Mudry and L. Dodelé, "History of the technological development of air conduction hearing aids," *J. Laryngology Otology*, vol. 114, no. 6, pp. 418–423, Jun. 2000.
[9] H. H. Kim and D. M. Barrs, "Hearing aids: A review of what's new," *J. Otolaryngol.-Head Neck Surg.*, vol. 134, no. 6, pp. 1043–1050, Jun. 2006.
[10] I. Mosnier, O. Sterkers, D. Bouccara, and S. Labassi, "Benefit of the vibrant soundbridge device in patients implanted for 5 to 8 years," *Ear Hearing*, vol. 29, no. 2, pp. 281–284, Apr. 2008.
[11] V. Colletti, S. D. Soli, M. Carner, and L. Colletti, "Treatment of mixed hearing losses via implantation of a vibratory transducer on the round window," *Int. J. Audiol.*, vol. 45, no. 10, pp. 600–608, Jan. 2006.
[12] J. M. Lee, J. Jung, I. S. Moon, S. H. Kim, and J. Y. Choi, "Benefits of active middle ear implants in mixed hearing loss: Stapes versus round window," *Laryngoscope*, vol. 127, no. 6, pp. 1435–1441, Jun. 2017.
[13] T. M. Eßinger, M. Koch, M. Bornitz, N. Lasurashvili, M. Neudert, and T. Zahnert, "Sensor-actuator component for a floating mass transducer-based fully implantable hearing aid," *Hearing Res.*, vol. 378, pp. 157–165, Jul. 2019.
[14] D. H. Shin and J.-H. Cho, "Design and development of a tri-coil bellows transducer for RW-drive implantable middle-ear hearing aid using FEA," *IEEE/ASME Trans. Mechatronics*, vol. 23, no. 3, pp. 1436–1444, Jun. 2018.
[15] E. Glennon, M. A. Svirsky, and R. C. Froemke, "Auditory cortical plasticity in cochlear implant users," *Current Opinion Neurobiol.*, vol. 60, pp. 108–114, Feb. 2020.
[16] Y. Xu, C. Luo, F.-G. Zeng, J. C. Middlebrooks, H. W. Lin, and Z. You, "Design, fabrication, and evaluation of a parylene thin-film electrode array for cochlear implants," *IEEE Trans. Biomed. Eng.*, vol. 66, no. 2, pp. 573–583, Feb. 2019.
[17] J. B. Firszt, L. K. Holden, R. M. Reeder, L. Cowdrey, and S. King, "Cochlear implantation in adults with asymmetric hearing loss," *Ear Hearing*, vol. 33, no. 4, pp. 521–533, 2012.
[18] B. Håkansson, S. Reinfeldt, M. Eeg-Olofsson, P. Östli, H. Taghavi, J. Adler, J. Gabrielsson, S. Stenfelt, and G. Granström, "A novel bone conduction implant (BCI): Engineering aspects and pre-clinical studies," *Int. J. Audiol.*, vol. 49, no. 3, pp. 203–215, Jan. 2010.
[19] R. Weiss, A. Loth, M. Leinung, S. Balster, D. Hirth, T. Stöver, S. Helbig, and S. Kramer, "A new adhesive bone conduction hearing system as a treatment option for transient hearing loss after middle ear surgery," *Eur. Arch. Oto-Rhino-Laryngol.*, vol. 277, no. 3, pp. 751–759, Mar. 2020.
[20] A. Canale, V. Boggio, A. Albera, M. Ravera, F. Caranzano, M. Lacilla, and R. Albera, "A new bone conduction hearing aid to predict hearing outcome with an active implanted device," *Eur. Arch. Oto-Rhino-Laryngol.*, vol. 276, no. 8, pp. 2165–2170, Aug. 2019.
[21] A. Magele, P. Schoerg, B. Stanek, B. Gradl, and G. M. Sprinzl, "Active transcutaneous bone conduction hearing implants: Systematic review and meta-analysis," *PLoS ONE*, vol. 14, no. 9, 2019, Art. no. e0221484.
[22] S. Reinfeldt, B. Håkansson, H. Taghavi, and M. Eeg-Olofsson, "New developments in bone-conduction hearing implants: A review," *Med. Devices (Auckland, NZ)*, vol. 8, pp. 79–93, Jan. 2015.
[23] D. H. Shin, K. W. Seong, E. S. Jung, J.-H. Cho, and K.-Y. Lee, "Design of a dual-coil type electromagnetic actuator for implantable bone conduction hearing devices," *Technol. Health Care*, vol. 27, pp. 445–454, Jun. 2019.
[24] F. A. Tietze, L. Hundertmark, M. Roy, M. Zerr, C. Sinke, D. Wiswede, M. Walter, T. F. Münte, and G. R. Szycik, "Auditory deficits in audiovisual speech perception in adult Asperger's syndrome: fMRI study," *Frontiers Psychol.*, vol. 10, p. 2286, Oct. 2019.
[25] V. M. Shklovsky, S. A. Varlamov, A. G. Petrushevsky, and L. A. Mayorova, "Speech and non-speech sound categorization in auditory cortex: FMRI correlates," *Human Physiol.*, vol. 45, no. 6, pp. 577–586, Nov. 2019.
[26] G. Bauernfeind, S. Haumann, and T. Lenarz, "FNIRS for future use in auditory diagnostics," *Current Directions Biomed. Eng.*, vol. 2, no. 1, pp. 229–232, Jan. 2016.
[27] J. Saliba, H. Bortfeld, D. J. Levitin, and J. S. Oghalai, "Functional near-infrared spectroscopy for neuroimaging in cochlear implant recipients," *Hearing Res.*, vol. 338, pp. 64–75, Aug. 2016.
[28] S. Harrison and D. Hartley, "Shedding light on the human auditory cortex: A review of the advances in near infrared spectroscopy (NIRS)," *Rep. Med. Imag.*, vol. 12, pp. 31–42, Oct. 2019.
[29] L. P. van de Rijt, M. M. van Wanrooij, A. F. Snik, E. A. Mylanus, A. J. van Opstal, and A. Roye, "Measuring cortical activity during auditory processing with functional near-infrared spectroscopy," *J. Hearing Sci.*, vol. 8, no. 4, pp. 9–18, Nov. 2018.
[30] A. M. Huber, J. H. Sim, Y. Z. Xie, M. Chatzimichalis, O. Ullrich, and C. Röösli, "The bonebridge: Preclinical evaluation of a new transcutaneously-activated bone anchored hearing device," *Hearing Res.*, vol. 301, pp. 93–99, Jul. 2013.
[31] D. H. Shin, K. W. Seong, S. Puria, K.-Y. Lee, and J.-H. Cho, "A tri-coil bellows-type round window transducer with improved frequency characteristics for middle-ear implants," *Hearing Res.*, vol. 341, pp. 144–154, Nov. 2016.
[32] B. Balachandran and E. B. Magrab, *Vibrations*. New York, NY, USA: Cambridge Univ. Press, 2018.
[33] H. Taghavi, B. Håkansson, and S. Reinfeldt, "A novel bone conduction implant-analog radio frequency data and power link design," in *Proc. 9th IASTED Int. Conf. Biomed. Eng.*, Innsbruck, Austria, 2012, pp. 327–335.
[34] G. J. Basura, X. S. Hu, J. S. Juan, A. M. Tessier, and I. Kovelman, "Human central auditory plasticity: A review of functional near-infrared spectroscopy (fNIRS) to measure cochlear implant performance and tinnitus perception," *Laryngoscope Investigative Otolaryngol.*, vol. 3, no. 6, pp. 463–472, Oct. 2018.
[35] H. Bortfeld, "Functional near-infrared spectroscopy as a tool for assessing speech and spoken language processing in pediatric and adult cochlear implant users," *Develop. Psychobiol.*, vol. 61, no. 3, pp. 430–443, Apr. 2019.
[36] S. Heinzel, F. B. Haeussinger, T. Hahn, A.-C. Ehlis, M. M. Plichta, and A. J. Fallgatter, "Variability of (functional) hemodynamics as measured with simultaneous fNIRS and fMRI during intertemporal choice," *NeuroImage*, vol. 71, pp. 125–134, May 2013.
[37] V. L. Towle, J. Bolaños, D. Suarez, K. Tan, R. Grzeszczuk, D. N. Levin, R. Cakmur, S. A. Frank, and J.-P. Spire, "The spatial location of EEG electrodes: Locating the best-fitting sphere relative to cortical anatomy," *Electroencephalogr. Clin. Neurophysiol.*, vol. 86, no. 1, pp. 1–6, Jan. 1993.
[38] K. E. Jang, S. Tak, J. Jung, J. Jang, Y. Jeong, and J. C. Ye, "Wavelet minimum description length detrending for near-infrared spectroscopy," *J. Biomed. Opt.*, vol. 14, no. 3, 2009, Art. no. 034004.
[39] J. Ye, S. Tak, K. Jang, J. Jung, and J. Jang, "NIRS-SPM: Statistical parametric mapping for near-infrared spectroscopy," *NeuroImage*, vol. 44, no. 2, pp. 428–447, Jan. 2009.

SEUNG HYUN LEE received the B.S. and M.S. degrees in electrical engineering and the Ph.D. degree in biomedical engineering from Kyungpook National University, South Korea, in 2006, 2008, and 2018, respectively.

From 2008 to 2018, he has spent his research period with the Daegu Gyeongbuk Institute of Science and Technology (DGIST). He was a Postdoctoral Researcher with the Institute of Biomedical Engineering Research, Kyungpook National University, in 2019. He is currently a Research Professor with Korea University, South Korea. His current research interests include functional near-infrared spectroscopy (fNIRS), neuroimaging, brain signal analysis, and machine learning.

KI WOONG SEONG received the B.S. degree in electronics engineering, in 1998, and the M.S. and Ph.D. degrees in electronics engineering from Kyungpook National University, Daegu, South Korea, in 2000 and 2010, respectively.

From 2010 to 2011, he was a Research Professor with the Institute of Biomedical Engineering Research, Kyungpook National University. Since 2012, he has been a Professor with the Department of Biomedical Engineering, Kyungpook National University Hospital, South Korea. His research interests include implantable hearing aids, bioelectronics, biomedical signal processing, and sensor applications in biomedical instrumentations

KYU-YUP LEE received the B.S. degree from the School of Medicine, in 1996, and the M.S. and Ph.D. degrees from the School of Medicine, Kyungpook National University, Daegu, South Korea, in 2003 and 2008, respectively.

From 2004, he has been a Professor with the Department of Otorhinolaryngology-Head and Neck Surgery, School of Medicine, Kyungpook National University. His research interests include hearing rehabilitation device, ear and mastoid disease, implantable bone conduction hearing aids, and sensor applications in biomedical instrumentations.

DONG HO SHIN received the B.S. degree in electronics engineering from Dongseo University, Busan, South Korea, in 2009, and the M.S. and Ph.D. degrees from the School of Electronics Engineering, Kyungpook National University, South Korea, in 2011 and 2016, respectively.

From 2016 to 2019, he was a Research Fellow with the Institute of Biomedical Engineering Research, Kyungpook National University, where he currently works as a Research Professor. His research interests include electronic and mechanical system of medical instruments and middle-ear implants transducer.